Han, X.; Franssens, J.; Rosolem, R.; Jiménez Bello, MA.; Bogena, H.; Martínez Alzamora, F.; Chanzy, A.... (2016). Simultaneous soil moisture and properties estimation for a drip irrigated field by assimilating cosmic-ray neutron intensity. Journal of Hydrology. 539:611-624. doi:10.1016/j.jhydrol.2016.05.050.

Simultaneous Soil Moisture and Properties Estimation for a Drip Irrigated Field by Assimilating Cosmic-ray Neutron Intensity

Xujun Han[1,2], Harrie-Jan Hendricks Franssen[1,2], Miguel Ángel Jiménez Bello[3], Rafael Rosolem[4], Heye Bogena[1], Fernando Martínez Alzamora[3], André Chanzy[5], Harry Vereecken [1,2]

1. Forschungszentrum Jülich, Agrosphere (IBG 3), Leo-Brandt-Strasse, 52425 Jülich, Germany
2. Centre for High-Performance Scientific Computing in Terrestrial Systems: HPSC TerrSys, Geoverbund ABC/J, Leo-Brandt-Strasse, 52425 Jülich, Germany
3. Institute of Water and Environmental Engineering (IIAMA). Universitat Politècnica de Valencia. Camino de Vera, s/n, 46022 Valencia, Spain
4. Department of Civil Engineering, University of Bristol, Bristol BS8 1TR, UK
5. INRA, UMR1114, Environnement Méditerranéen et Modélisation des AgroHydrosystèmes, Domaine Saint Paul, Site Agroparc, F-84914 Avignon, France

Corresponding author: Xujun Han, Forschungszentrum Jülich, Agrosphere (IBG 3), Leo-Brandt-Strasse, 52425 Jülich, Germany. (x.han@fz-juelich.de)

Abstract

Neutron intensity measured by the aboveground cosmic-ray neutron intensity probe (CRP) allows estimating soil moisture content at the field scale. In this work, synthetic neutron intensities were used to remove the bias of simulated soil moisture content or update soil hydraulic properties (together with soil moisture) in the Community Land Model (CLM) using the Local Ensemble Transform Kalman Filter. The cosmic-ray forward model COSMIC was used as the non-linear measurement operator which maps between neutron intensity and soil moisture. The novel aspect of this work is that synthetically measured neutron intensity was used for real time updating of soil states and soil properties (or soil moisture bias) and posterior use for the real time scheduling of irrigation (data assimilation based real-time control approach). Uncertainty of model forcing and soil properties (sand fraction, clay fraction and organic matter density) were considered in the ensemble predictions of the soil moisture profiles. Horizontal and vertical weighting of soil moisture was introduced in the data assimilation in order to handle the scale mismatch between the cosmic-ray footprint and the CLM grid cell.

The approach was illustrated in a synthetic study with the real-time irrigation scheduling of fields of citrus trees. After adjusting soil moisture content by assimilating neutron intensity, the irrigation requirements were calculated based on the water deficit method. Model bias was introduced by using coarser soil texture in the data assimilation experiments than in reality. A series of experiments was done with different combinations of state, parameter and bias estimation in combination with irrigation scheduling.

Assimilation of CRP neutron intensity improved soil moisture characterization. Irrigation requirement was overestimated if biased soil properties were used. The soil moisture bias was reduced by 35% after data assimilation. The scenario of joint state-parameter estimation resulted in the best soil moisture characterization (50% decrease in root mean square error compared to open loop simulations), and the best estimate of needed irrigation amount (86% decrease in Hausdorff distance compared

to open loop). The coarse scale synthetic CRP observation was proven to be useful for the fine scale soil moisture and soil properties estimation for the objective of irrigation scheduling.

Keywords: Data Assimilation; Cosmic ray; Soil Moisture; Parameter Estimation; Bias Estimation; Irrigation Scheduling

1. Introduction

Globally, 70% of fresh water is used by agriculture (FAO - Food and Agriculture Organization of the United Nations). Therefore, it is necessary to increase the water use efficiency and reduce the water need for crop production, while maintaining crop yield. Enough water should be applied to meet the requirement of maximum crop evapotranspiration (ET). Farmers usually base irrigation scheduling on their own experience taking into account soil water status and crop growth. However, it is unlikely that the optimal scheduling of irrigation is acquired without the knowledge of crop water needs. Low cost sensors that measure soil moisture content can be of advantage. However, these sensors typically have a very small measurement volume which is much smaller than the scale of the fields where the crops are grown. Numerical models like crop growth models (Heng et al., 2009) and land surface models (Wood et al., 2011) can be used for the quantitative estimation of the irrigation requirement under specific soil water and crop growth conditions. The estimated irrigation amount can be applied accurately with new agricultural technology like drip irrigation (Sampathkumar et al., 2012). However, uncertain model input data and deficits in the model structure result in biased estimates of soil water status, crop transpiration and therefore irrigation requirement.

The optimal scheduling of irrigation is complicated given the high heterogeneity of soil moisture content in drip irrigated fields. An estimate of soil moisture content for the complete root zone is important in this context. It is difficult to achieve this with small-scale measurements (e.g., TDR-Time Domain Reflectometry,

77 FDR-Frequency Domain Reflectometry or TDT-Time Domain Transmission) as a
78 prohibitively large number of sensors is needed to cover large irrigated areas. Soil
79 moisture information from remote sensing on the other hand is limited to the upper
80 few soil centimeters, and often has a very coarse horizontal resolution (>10 km)
81 (Entekhabi et al., 2010; Kerr et al., 2010; Montzka et al., 2013). A further limitation
82 of satellite-derived soil moisture content is that it is not reliable for highly vegetated
83 areas (Njoku and Chan, 2006) and high uncertainties (Merlin et al., 2009; Montzka et
84 al., 2013). The spatial variability of soil moisture is controlled by soil hydraulic
85 properties, meteorological forcing, land cover patterns and topographic features at
86 different measurement scales. Small scale variability is more driven by soil hydraulic
87 properties while large scale variability is also more driven by the other factors. Hence,
88 strengths and weaknesses of each measurement method rely on the additional
89 uncertainty given by these additional controlling factors (Crow et al., 2012).

90 A new promising method which can determine integral root zone soil moisture
91 from the measured above ground fast neutron intensity (defined as the number of
92 counted neutrons per unit of time – e.g., counts per hour) has been proposed (Zreda et
93 al., 2012). This synthetic study focuses on the assimilation of cosmic-ray probe (CRP)
94 neutron intensity (Bogena et al., 2013; Desilets et al., 2010; Rosolem et al., 2014;
95 Shuttleworth et al., 2013; Zreda et al., 2008; Zreda et al., 2012). Soil moisture
96 measurements at the intermediate scale of the cosmic ray probe have the advantage
97 that they are less affected by small scale variability of soil hydraulic properties. A
98 further advantage is that soil moisture can be determined for a deeper layer (10-70 cm)

99 in higher temporal frequency than remote sensing (Rosolem et al., 2014).

100 Primary cosmic rays originate from our galaxy and eventually collide with
101 atmospheric nuclei, generating secondary cosmic rays mainly consisting of neutrons
102 (Lal and Peters, 1967). Primary cosmic rays create cascades of secondary high-energy
103 neutrons through colliding with atmospheric nuclei and the high-energy neutrons can
104 penetrate the atmosphere and collide with nuclei in soils. These collisions in the soil
105 generate fast neutrons. Some of these fast neutrons are eventually scattered back to
106 the atmosphere and the fast neutron intensity can be measured with the CRP. The
107 measured intensity of fast neutrons above the ground depends strongly on soil
108 moisture content (Hendrick and Edge, 1966; Zreda et al., 2012). CRPs make use of
109 this principle to estimate soil moisture content for an area of about 600 m diameter
110 and variable measurement depth (~10-70 cm) depending on the soil moisture
111 conditions (Zreda et al., 2012).

112 Measured neutron intensities above ground need to be corrected for variations in
113 incoming high-energetic neutrons and atmospheric pressure (Zreda et al., 2012).
114 Moreover, as the measured neutron intensity depends on additional sources of
115 hydrogen (besides of soil moisture), these need to be taken into account in order to
116 isolate the soil moisture signal. Corrections have been proposed for other hydrogen
117 sources like atmospheric vapor (Rosolem et al., 2013), lattice water and organic
118 carbon in the soil (Franz et al., 2013), hydrogen atoms stored in the litter layer
119 (Bogena et al., 2013) and above-ground biomass (Baatz et al., 2015). Data
120 assimilation studies have shown the advantage of using measured multi-source soil

moisture observations for improving the soil moisture profile characterization of a land surface model (Crow et al., 2008; De Lannoy et al., 2007b; Han et al., 2012; Huang et al., 2008; Reichle et al., 2008; Walker et al., 2001). Measured neutron intensities have already been used for assimilation in a land surface model to improve estimates of soil moisture profiles, but the model parameters were calibrated a priori (Han et al., 2015a; Rosolem et al., 2014; Shuttleworth et al., 2013).

In this paper we will investigate the benefits of assimilating coarse scale (600 m) neutron intensity data into the Community Land Model (CLM) for the application of drip irrigation for citrus trees on a finer scale (100 m) than the CRP scale. The neutron intensity measured by a synthetic CRP affects a larger area than a typical irrigation management unit (1 ha in this work). In order to study the impact of soil moisture data assimilation on irrigation scheduling, the drip irrigation was therefore simulated at a finer spatial scale than the footprint of a CRP. The drip irrigation was applied at the vegetated area and resulted in a very heterogeneous soil moisture distribution with the alternation of patches of wet and dry soil. It is very CPU-intensive to explicitly model the irrigated patches and the non-irrigated parts, and a simplified implementation was adopted in this work, which will be further detailed in the methodology section. In the simulation experiments, CLM was driven by biased soil properties to mimic the intrinsic model uncertainties. The coarse scale CRP neutron intensity observations were used to update the field scale heterogeneous soil moisture field through data assimilation. The joint soil moisture and soil properties (or soil moisture bias) estimation scheme was evaluated. This is important because soil moisture content and

crop transpiration are sensitive to model parameters (Hou et al., 2012; Rosolem et al., 2012; Schwinger et al., 2010). Typically, field measurements of parameter values are scarce and very uncertain, especially because of the scale mismatch between a local measurement and the model scale (Waller et al., 2014). Model parameter estimation in the context of a data assimilation framework was proven to be successful, using either an augmented state vector approach (Chen and Zhang, 2006), dual state parameter estimation (Moradkhani et al., 2005b) or parameter estimation in a loop external to the data assimilation filter (Vrugt et al., 2005). Successful applications are reported for such diverse areas as groundwater hydrology (Franssen and Kinzelbach, 2008; Kurtz et al., 2014; Schöniger et al., 2012), rainfall-runoff models (Moradkhani et al., 2005a; Vrugt et al., 2006), land surface models (Han et al., 2014a; Pauwels et al., 2009), vadose zone hydrology (Montzka et al., 2011; Wu and Margulis, 2013) and atmospheric models (Ruiz et al., 2013). A data assimilation framework can consider uncertain model forcing, model structure and initial conditions, as well as parameter uncertainties. Data assimilation has become a commonly used method for parameter estimation, especially for large scale applications (Wanders et al., 2014).

Joint soil moisture and soil moisture bias estimation has been proven to be helpful for improving data assimilation results (De Lannoy et al., 2007a; Kumar et al., 2012b) like soil temperature assimilation with bias correction (Bosilovich et al., 2007; Reichle et al., 2010). In this study, we also evaluated the impact of the soil moisture bias estimation method (Dee, 2005) on improving the soil moisture assimilation and irrigation scheduling and compared it with joint state-parameter estimation.

It is expected that a more accurate characterization of the heterogeneous soil moisture distribution can be obtained if the coarse scale CRP neutron intensity data are assimilated using a combination of data assimilation and parameter estimation (or bias estimation). Based on such results, it is then assumed that the estimated irrigation requirement could be improved. The objective of this study is to evaluate with help of a synthetic study: 1) the potential of measured neutron intensity data by the CRP for improving the characterization of soil moisture content and soil properties (or soil moisture bias), and 2) the impact of the assimilation of neutron intensity on better irrigation scheduling and the potential for real-time irrigation optimization. In this study, the spatial variability of soil properties and crop status will be considered in the data assimilation.

2. Methodology

The main components of the methodology are: (i) measurement of above-ground neutron intensity, which is linked to field scale soil moisture content by a measurement operator (section 2.1) and horizontal weights (section 2.3); (ii) the land surface model CLM (version 4.5) which simulates the transport of water and energy in the soil-plant-atmosphere continuum (section 2.2); (iii) data assimilation according to the Local Ensemble Transform Kalman Filter (LETKF) methodology (Hunt et al., 2007) which optimally combines measurements and model predictions to update soil moisture (and possibly soil properties or soil moisture bias), taking into account uncertain atmospheric forcing and model parameters (or model bias) (section 2.3) and

187 (iv) an optimization routine which calculates irrigation need for the ensemble of soil
188 moisture forecasts (section 2.4).

189 **2.1. Cosmic ray Soil Moisture Interaction Code (COSMIC)**

190 In order to assimilate neutron intensity, the relationship between neutron intensity
191 and depth-weighted soil moisture content should be reasonably represented. The
192 newly-developed COsmic ray Soil Moisture Interaction Code (COSMIC)
193 (Shuttleworth et al., 2013) was adopted as the forward observation operator to
194 simulate the equivalent neutron count rates from simulated soil moisture profiles (i.e.,
195 soil moisture contents for 10 vertical model layers of CLM from surface to 3 m depth,
196 in this study) and takes into account the weighted contribution of individual soil
197 layers with depth. The COSMIC operator calculates the number of fast neutrons
198 reaching the CRP N_{COSMOS} at a near-surface measurement point by:

199 $$N_{COSMOS} = N\int_0^{\infty}\left\{A(z)[\alpha\rho_s(z)+\rho_w(z)]\exp\left(-\left[\frac{m_s(z)}{L_1}+\frac{m_w(z)}{L_2}\right]\right)\right\}dz \quad (1)$$

200 $$A(z) = \left(\frac{2}{\pi}\right)\int_0^{\pi/2}\exp\left(\frac{-1}{\cos(\varphi)}\left[\frac{m_s(z)}{L_3}+\frac{m_w(z)}{L_4}\right]\right)d\varphi \quad (2)$$

201 $$\alpha = 0.405 - 0.102 \times \rho_s \quad (3)$$

202 $$L_3 = -31.76 + 99.38 \times \rho_s \quad (4)$$

203 where N (counts/h) is the number of high-energy neutrons at the soil surface, z
204 is the soil layer depth (m), ρ_s is the dry soil bulk density (g cm^{-3}), ρ_w is the total
205 soil water density, including the lattice water (g cm^{-3}); $m_s(z)$ and $m_w(z)$ are the
206 integrated mass per unit area of dry soil and water (g cm^{-2}), φ is the angle between
207 the vertical below the detector and the line between the detector and each point in the

208 plane (Shuttleworth et al., 2013), L_1 is the high energy soil attenuation length with
209 value of 162.0 gcm^{-2}, L_2 is the high energy water attenuation length of 129.1 gcm^{-2},
210 L_3 is the fast neutron soil attenuation length (gcm^{-2}) and L_4 is the fast neutron water
211 attenuation length with value of 3.16 gcm^{-2} (Shuttleworth et al., 2013).

212 In this study soil moisture contents for 10 vertical soil layers of CLM were used
213 to drive the COSMIC operator. COSMIC interpolates the soil moisture to 300 layers
214 with a soil profile depth of 3 meters and derives the fast neutron count rate from the
215 depth-averaged soil moisture content based on the effective sensor depth, also
216 calculated by COSMIC. The simulated fast neutron intensity was assumed to be
217 observed and subsequently used for the data assimilation as will be explained below.
218 Vertical variation of soil moisture content will be considered according to the
219 contribution to the total neutron intensity of each soil layer.

220

221 **2.2. Community Land Model - CLM**

222 The Community Land Model (CLM - version 4.5) developed by the National
223 Center for Atmospheric Research (NCAR) was used to calculate soil moisture content
224 and evapotranspiration (Oleson et al., 2013). CLM uses the simplified Richards
225 equation to model water flow in the unsaturated zone and calculation of land surface
226 energy fluxes is done by invoking the Monin-Obukhov similarity theory. In addition,
227 the following processes can be simulated by CLM: transfer of solar radiation and
228 longwave radiation, stomatal physiology and photosynthesis, crop dynamics and
229 irrigation (Oleson et al., 2013). The land cover can be represented by 17 plant

functional types (PFTs) and the calculation of energy fluxes is based on the PFTs. Hydraulic and thermal parameters in CLM are derived based on soil properties such as sand and clay fraction and organic matter density (Oleson et al., 2013).

2.3. Data Assimilation and Parameter Estimation

The Local Ensemble Transform Kalman Filter (LETKF) is a square root ensemble Kalman filter (Hunt et al., 2007; Miyoshi and Yamane, 2007), which is applied extensively in atmospheric data assimilation studies (Aravéquia et al., 2011; Baek et al., 2006; Lien et al., 2013; Miyoshi et al., 2014) and also in land data assimilation studies (Han et al., 2014a). In LETKF, the uncertainty of the model forecast is represented by ensemble members. In this study LETKF is used to estimate both soil moisture and soil properties with the state augmentation method (Bateni and Entekhabi, 2012; Han et al., 2014a; Li and Ren, 2011) or to update soil moisture and soil moisture bias jointly.

First two matrices $\mathbf{X}^b$ and $\mathbf{Y}^b$ are constructed based on simulated soil moisture and soil properties (or soil moisture bias) of the ensemble members:

$$\mathbf{X}^b = \left[\mathbf{x}_1^b - \overline{\mathbf{x}}^b, \ldots, \mathbf{x}_M^b - \overline{\mathbf{x}}^b\right] \quad (5)$$

$$\mathbf{y}_i^b = H\left(\mathbf{x}_i^b\right) \quad (6)$$

$$\mathbf{Y}^b = \left[\mathbf{y}_1^b - \overline{\mathbf{y}}^b, \ldots, \mathbf{y}_M^b - \overline{\mathbf{y}}^b\right] \quad (7)$$

where $\mathbf{x}_1^b, \ldots \mathbf{x}_M^b$ are vectors with the ensemble members, M is the ensemble size, $\overline{\mathbf{x}}^b$ is the vector with ensemble means calculated over $\mathbf{x}_1^b, \ldots \mathbf{x}_M^b$, H is the observation operator (i.e., COSMIC for soil moisture), $\mathbf{y}_i^b$ is the mapping of the

ensemble members $\mathbf{x}_1^b,\ldots\mathbf{x}_M^b$ to the measurement space and $\bar{\mathbf{y}}^b$ is the vector of ensemble means of $\mathbf{y}_1^b,\ldots\mathbf{y}_M^b$. The vector $\bar{\mathbf{x}}^b$ contains i) the depth weighted average soil moisture θ_{cosmic}, which was derived from COSMIC and considers the contribution of different soil layers, ii) the soil moisture of 10 layers ($\theta_1\ldots\theta_{10}$) and iii) soil properties (sand fraction, clay fraction and organic matter density) in case soil properties are estimated. In case of bias estimation, the vector $\bar{\mathbf{x}}^b$ contains soil moisture bias instead of soil properties. The dimensions of the augmented state vector $\bar{\mathbf{x}}^b$ were 11 for the state estimation only, 14 for joint state and parameter estimation, and 12 for joint state and bias estimation. Only soil properties and soil moisture bias for the upper soil layer were included in the state vector $\bar{\mathbf{x}}^b$. Soil properties for all 10 layers were updated based on the ratio of the soil properties between the upper soil layer and the lower soil layers (Han et al., 2014b). The soil moisture bias of deeper layers was assumed to decrease exponentially according to equation (8).

$$\bar{\mathbf{x}}^b = \left\{ \begin{array}{ll} \begin{bmatrix} \theta_{cosmic} \\ \theta_1 \\ \vdots \\ \theta_{10} \end{bmatrix} & state\,estimation \\ \begin{bmatrix} \theta_{cosmic} \\ \theta_1 \\ \vdots \\ \theta_{10} \\ Sand \\ Clay \\ Organic \end{bmatrix} & parameter\,estimation \\ \begin{bmatrix} \theta_{cosmic} \\ \theta_1 + \theta_{Bias}^{k-1} * exp\left(-1.0 * Z_1\right) \\ \vdots \\ \theta_{10} + \theta_{Bias}^{k-1} * exp\left(-1.0 * Z_{10}\right) \\ \theta_{Bias}^{k-1} \end{bmatrix} & bias\,estimation \end{array} \right\} \tag{8}$$

where Z_i (m) is the i^{th} soil layer thickness of CLM and k is the time step.

Next, the analysis error covariance matrix $\mathbf{P}^a$ is calculated:

$$\mathbf{P}^a = \left[\left(M-1\right)\mathbf{I} + \mathbf{Y}^{bT}\mathbf{R}^{-1}\mathbf{Y}^b \right] \tag{9}$$

where $\mathbf{R}$ is the observation error covariance matrix. The perturbations in the ensemble space $\mathbf{W}^a$ are calculated according to:

$$\mathbf{W}^a = \left[\left(M-1\right)\mathbf{P}^a \right]^{1/2} \tag{10}$$

The analysis mean $\bar{\mathbf{w}}^a$ is given by:

$$\bar{w}^a = \mathbf{P}^a\mathbf{Y}^{bT}\mathbf{R}^{-1}\left(\mathbf{y}^o - \bar{\mathbf{y}}^b\right) \tag{11}$$

where $\mathbf{y}^o$ is the vector with the measured CRP neutron intensity. The analysis mean is added to each column of $\mathbf{W}^a$ to get the analysis ensemble.

Finally, the new analysis $\mathbf{X}^a$ is obtained according to:

$$\mathbf{X}^a = \mathbf{X}^b\mathbf{W}^a + \bar{\mathbf{x}}^b \tag{12}$$

where $\mathbf{X}^a$ are the model ensemble members after analysis. $\mathbf{X}^a$ includes the updated soil moisture and soil properties (or soil moisture bias), and will be used as initial condition for the next time step.

The forecast model of soil moisture bias $\boldsymbol{\theta}_{Bias}^{k}$ was defined as:

$$\boldsymbol{\theta}_{Bias}^{k} = \boldsymbol{\theta}_{Bias}^{k-1} \tag{13}$$

where k is the time step.

In this study, the LETKF was applied as a 1D filter to update soil moisture in the cosmic ray footprint, which covered several fine scale model grid cells. Neutron intensity data were used to update the fine scale soil moisture within the expected CRP footprint and the contribution of different grid cells within the CRP footprint to the observed neutron intensity was taken into account by assigning different horizontal weights to the CLM grid cells. Following the horizontal weighting method proposed by (Bogena et al., 2013), we used a Gaussian window function (Harris, 1978) to define the horizontal weights of the different CLM grid cells in the CRP footprint. Because a single observation was used to update the soil moisture content of many CLM grid cells, a simple multi-scale data assimilation strategy was proposed. First, the COSMIC operator was run for each CLM grid cell to simulate the neutron intensity of each CLM grid cell. Next, a convolution with a Gaussian window function was applied to retrieve the integrated neutron intensity at the coarse scale. This convolution step was used in both the ensemble runs and the parallel runs (introduced in section 3.3). Therefore the CRP neutron intensity (measured/simulated) considered the contributions from all model grid cells contained within the CRP

footprint. The size of the Gaussian window function was chosen as the diameter of the CRP footprint (600 m). The observation operator *H* (needed by equation (6)) was defined as the combination of a Gaussian window function and the COSMIC operator. Using equation (6) we get:

$$\mathbf{y}_i^b = f_{Gaussian}(f_{cosmic}\left(\mathbf{x}_i^b\right)) \quad (14)$$

where f_{cosmic} represents the COSMIC operator and $f_{Gaussian}$ the Gaussian window function.

The footprint of the CRP covered 43 CLM grid cells (i.e., ~600 m diameter). The data assimilation was done grid cell by grid cell in LETKF. Therefore the time series of a single neutron intensity observation was assigned uniformly to all grid cells of the CRP footprint and then the observations were assimilated separately for each CLM grid cell. The spatial localization was applied on the model states using equation (14), and therefore the observation localization was not used in this study (Greybush et al., 2011; Han et al., 2015b). The soil moisture measured by CRP is composed of the contribution of all horizontal and vertical CLM grid cells of the CRP footprint. Therefore, there is only one relevant soil moisture content value and neutron intensity value. Given equation (14), the upscaling of soil moisture from CLM will be done before assimilation, it means the upscaled soil moisture θ_{cosmic} which incorporates the contribution from all surrounding grid cells will be used as the soil moisture content value to be updated with the CRP neutron intensity measurement. All the soil moisture content values for the individual grid cells within the CRP footprint (both horizontally and vertically) will be updated according to the correlation between the

simulated values by CLM and θ_{cosmic}:

$$\theta_{cosmic} = f_{Gaussian}(f_{cosmic}(\mathbf{x}_i^b)) \quad (15)$$

2.4. Irrigation Requirement

CLM computes the water deficit between the current soil moisture content and a target soil moisture content. The target soil moisture in each soil layer is a weighted average of (1) the minimum needed soil moisture content to avoid water stress for that layer and (2) the saturated soil moisture content for that layer (Levis and Sacks, 2011):

$$\theta_{target,i} = (1-0.7)\times\theta_{o,i} + 0.7\times\theta_{sat,i} \quad (16)$$

where i is the soil layer number, $\theta_{o,i}$ is the minimum soil moisture content of each vegetation type so that stomata are completely opened and $\theta_{sat,i}$ is the effective soil porosity.

The total water deficit $W_{deficit}$ (mm) was defined as:

$$W_{deficit} = \sum_{i}^{N} Root\_Fraction_i \times \max(\theta_{target,i} - \theta_{liq,i}, 0) \quad (17)$$

where $\theta_{liq,i}$ is the current soil moisture content of layer i.

The estimated irrigation amount $W_{deficit}$ was applied in CLM as an incoming water flux not subjected to interception by the canopy layer (precipitation on the contrary was subjected to interception).

The root fraction (RF_i) of citrus trees for the soil layer i was parameterized as (Oleson et al., 2013):

$$RF_i = \begin{cases} 0.5\left[\begin{array}{c}\exp\left(-r_a Z_{h,i-1}\right)+\exp\left(-r_b Z_{h,i-1}\right)\\ -\exp\left(-r_a Z_{h,i}\right)+\exp\left(-r_b Z_{h,i}\right)\end{array}\right] & 1 \le i < N_{levsoi} \\ 0.5\left[\exp\left(-r_a Z_{h,i-1}\right)+\exp\left(-r_b Z_{h,i-1}\right)\right] & i = N_{levsoi} \end{cases} \quad (18)$$

where $Z_{h,i}$ (m) is the depth from the soil surface to the interface between soil layers i and $i+1$ ($Z_{h,0}=0$ represents the soil surface), r_a and r_b are plant dependent root distribution parameters, for citrus trees: $r_a = 8.992$, $r_b = 8.992$ (Zeng, 2001), $N_{levsoi} = 10$ is the total number of soil layers.

2.5. Performance Measures

In order to evaluate the results of data assimilation and irrigation, the Root Mean Square Error (RMSE) was calculated for the hourly soil moisture results:

$$\mathrm{RMSE} = \sqrt{\frac{\sum_{k=i}^{K}\left(\theta_{est} - \theta_{ref}\right)^2}{K}} \quad (19)$$

where θ_{est} is the hourly soil moisture ensemble mean for a given scenario, θ_{ref} is the hourly soil moisture value of the reference scenario. K is equal to 8760. Soil moisture contents at the time points of assimilation and prediction were included in the calculations with Eq. 19. Lower RMSE values mean better performance.

The Hausdorff Distance (HD) is a quantitative measure of the similarity between two spatial distributions (Kumar et al., 2012a). Lower HD values mean higher spatial similarity. HD is defined as the maximum distance of a set to the nearest point in the other set:

$$h(Q,R) = \max_{q \in Q}\left\{\min_{r \in Q}\{q-r\}\right\} \quad (20)$$

where $h(Q,R)$ is the HD value and q and r are the points of sets Q and

363 R. $q-r$ is the norm of the points in the space of Q and R, in terms of Euclidean
364 distance. Q is the estimated annual irrigation amount of a CLM grid cell in the CRP
365 footprint and R is the annual irrigation amount of the reference scenario of the CRP
366 footprint.

367 The t-test can be used to determine whether two data sets are significantly
368 different. The independent two-sample t-test was used to evaluate the statistical
369 significance of the difference between the estimated irrigation amount and the
370 reference irrigation amount (Welch, 1947). The definition of the t-test is as follows:

371 $$t = \frac{\bar{X}_1 - \bar{X}_2}{\sqrt{\frac{s_1^2}{N_1} + \frac{s_2^2}{N_2}}} \quad (21)$$

372 where $\bar{X}_1 / \bar{X}_2$, s_1^2 / s_2^2 and N_1 / N_2 are the mean, variance and the number of
373 optimized irrigation amounts, respectively. The subscripts 1 and 2 represent the
374 reference scenario and estimation scenario, respectively.

375

376 **3. Synthetic Experiment**

377 A synthetic study was conducted to evaluate the methodology outlined in the
378 previous sections. The synthetic study mimicked the Picassent site (close to Valencia,
379 Spain) with citrus trees, which receives drip irrigation. The site is situated in a
380 semi-arid region (39.38^o N, 0.47^o E) with yearly average precipitation of 454 mm (44
381 precipitation days), average daily maximum temperature of 22.3^{o}C and average daily
382 minimum temperature of 13.4^{o}C, and with a yearly irrigation period from April to
383 October. In the synthetic experiments, a CRP (Zreda et al., 2012) measured the

384 neutron intensity which was assimilated in the land surface model CLM.

385

386 **3.1. Design of Synthetic Experiments**

387 The citrus tree was modeled as a broadleaf evergreen tropical PFT in CLM. In
388 order to mimic the planting pattern of citrus trees at the Picassent site, odd CLM grid
389 columns were modelled as bare ground without vegetation cover while even CLM
390 columns were modelled as fully covered by broadleaf evergreen tropical trees. The
391 mimicked ground cover of vegetation was similar to the real measured ground cover
392 fraction of citrus trees. Soil properties (sand fraction and clay fraction) and organic
393 matter density determine the soil thermal and hydraulic properties in CLM. Soil
394 samples from the Picassent region were taken and a soil sand fraction of 32%, clay
395 fraction of 33%, bulk density of 1.5 gcm^{-3}, and organic fraction of 1.2% (10 cm depth)
396 and 0.7% (50 cm depth) were determined and applied uniformly in space in CLM.
397 Spatially correlated noise was added to the uniform soil properties to represent the
398 spatial heterogeneity. The noise was simulated by sequential Gaussian simulation with
399 a correlation range of 100 m, variance of 100.0 (%) and mean value of 0.0 (%). The
400 noise was constrained within the range of (-5.0%, 5.0%) after the sequential Gaussian
401 simulation. The atmospheric forcing data measured by the Picassent weather station
402 were used as CLM input. The maximum rate of carboxylation at 25 ℃ (V_{cmax25})
403 controls the maximum rate of carboxylation and canopy transpiration in CLM. The
404 default value of V_{cmax25} is 55 $\mu molm^2s^{-1}$ for broadleaf evergreen tropical tree in
405 CLM. It was changed to 100 $\mu molm^2s^{-1}$ according to a reference value for citrus trees

406 (Velikova et al., 2012). The study area was discretized in 40×60 grid cells at a spatial
407 resolution of 100 m. However, our analysis will focus on the CRP footprint which
408 contains only 43 CLM grid cells in total. Because of the spatial discretization, it is not
409 easy to describe the exact CRP footprint. The diameter of the CRP footprint for the
410 horizontal weighting calculation was chosen as the ratio between the CRP diameter
411 and the spatial resolution of the CLM grid cell, which was 7 grid cells.

412 A model spin-up was made to obtain reasonable initial conditions for CLM. CLM
413 was run for the spin-up period from 2010-01-01 to 2010-12-31 using an hourly time
414 step. Next, a one-year (2011-01-01 to 2011-12-31) irrigation estimation using the true
415 soil properties was performed in CLM and the irrigation requirement was calculated
416 every three days during the period from 2011-01-01 to 2011-12-31 and subsequently
417 applied. This reference model run also supplied the reference soil moisture
418 distribution in space and time and the canopy transpiration, and a distribution in space
419 and time (and total amounts) of irrigation.

420

421 **3.2. Ensemble Generation**

422 The simulation experiments evaluated how well the soil moisture,
423 evapotranspiration, soil properties and irrigation requirement could be characterized if
424 soil properties and model forcing were biased and/or uncertain, but the measurement
425 data (albeit synthetically generated for this study) in the form of CRP neutron
426 intensity were available. We assumed that the soil texture was systematically coarser
427 than in reality. The soil properties used in the reference run were perturbed to

represent these conditions: the sand fraction was multiplied by 1.5 while the clay fraction and organic matter density were both multiplied by 0.75. In addition, for all scenarios the sand and clay fractions, and organic matter density were perturbed by a uniform distributed noise in the range of [-10.0%, 10.0%] (for soil texture) and [-10.0 km m^{-3}, 10.0 km m^{-3}] (for organic matter density) to generate 20 different soil hydraulic properties for the 20 different ensemble members. It is assumed that these perturbations represent a realistic representation of the uncertainty in practice. If the sum of the sand and clay fraction was larger than 98%, an amount equal to ((Sand%+Clay%) – 98%)/2.0 was subtracted from both the sand and the clay fraction. For the ensembles for which initial soil moisture bias was updated instead of soil properties, soil moisture was perturbed with a spatially uniform value sampled from the uniform distribution with values between -0.04 m^3m^{-3} and 0.04 m^3m^{-3}.

The atmospheric forcing data of precipitation, air temperature, shortwave incident radiation and longwave incident radiation were perturbed with a noise correlated in space and time (Han et al., 2013). The spatially correlated noise was generated using the Fast Fourier Transform approach and the temporal correlation was imposed by a first-order auto-regressive model approach (Kumar et al., 2009; Park and Xu, 2009). The perturbation parameters are summarized in Table 1.

3.3. Synthetic Observation

In this study, the “observed” synthetic CRP neutron intensity was generated using the COSMIC model, which used the soil moisture profile simulated by CLM as input.

A point which had to be considered in the simulation scenarios was that the soil moisture changed also as response to the irrigation amount applied in the CLM simulation. Therefore, the synthetic observations will be different for each simulation scenario due to the different irrigation amounts. In order to obtain the synthetic measurements of CRP neutron intensity for these scenario runs, a parallel run was made with the same soil properties and atmospheric forcing as the reference run for each of the simulation scenarios. However, the irrigation amount for this parallel run was the same as the optimized one for the specific simulation scenario. Therefore irrigation amounts differed among the parallel runs of the different scenarios. This in turn also affected the CRP intensity which was assimilated in the simulation scenarios. The soil moisture calculated in the parallel run was used now as the synthetic soil moisture measurement for this specific scenario and also used as input for COSMIC to estimate the synthetic CRP neutron intensity. This implies that the assimilated CRP neutron intensity differed among different scenarios, in correspondence with different irrigation amounts applied in the different scenarios.

In this synthetic study, N_{COSMOS} was set to 150 counts h^{-1} and lattice water was 3% in COSMIC. The simulated CRP intensity measurements were perturbed in order to represent the observation error. This perturbation had a mean equal to zero and a variance equal to the square root of the neutron intensity to represent the observation error. The CLM grid cells located in the footprint of the CRP were updated by the data assimilation procedure. The neutron intensity observation was assimilated at 23:00 each three days, prior to irrigation scheduling.

472 Fig. 1 shows a schematic overview of the complete calculation procedure for each
473 time step.
474 [Insert Figure 1 here]
475
476 **3.4. Irrigation Scheduling**
477 In Valencia, citrus trees are typically irrigated 3~6 days per week from April to
478 October. For simplicity, the irrigation duration was assumed to be two hours from
479 06:00 AM onwards, and the irrigation was applied every three days for reasons of
480 computational efficiency. CLM was run in prediction mode for three days to estimate
481 the needed amount of irrigation (at 06:00) using the predefined atmospheric forcing
482 data. The first assimilation of soil moisture data was done at 23:00, seven hours
483 before the start of the second irrigation period.
484 Five irrigation estimation scenarios were designed to assimilate the CRP neutron
485 intensity in the land surface model and to evaluate the impact of data assimilation,
486 parameter estimation and bias estimation on the characterization of the soil moisture
487 profile, irrigation amount and evapotranspiration:
488 (1) Irrigation estimation with the true soil properties and atmospheric forcing
489 (Reference).
490 (2) Irrigation estimation with biased soil properties, without CRP neutron
491 intensity assimilation (No_DA, i.e. Open loop).
492 (3) Irrigation estimation with biased soil properties, with the assimilation of CRP
493 neutron intensity (every three days) (Only_DA_SM).

(4) Irrigation estimation with biased soil properties, with both CRP neutron intensity assimilation (every three days) and soil moisture bias estimation (DA_SM_Bias).

(5) Irrigation estimation with biased soil properties, with neutron intensity assimilation (every three days) including soil properties estimation (DA_SM_Par). For the scenario of DA_SM_Par, the study period included both 2010 and 2011. In 2010, joint soil moisture and soil properties estimation were carried out in order to update the biased soil properties (sand fraction, clay fraction and organic matter density). Next, in 2011 the updated soil properties were used for soil moisture assimilation without soil properties updating. For the scenarios without soil properties estimation, the experiments were only carried out for 2011.

The estimation of soil properties during the year 2010 deteriorated in case of intensive irrigation. In case of intensive irrigation, the soil column is close to saturation, and the ensemble members show a limited spread. In addition, the sensitivity of soil moisture with respect to soil properties becomes small. Parameter estimation (i.e., updating of soil properties) is not very efficient during these periods. Therefore, soil properties were not updated if the accumulated irrigation amount between two data assimilation time steps was larger than 10 mm.

4. Results

In this section we evaluate time series for the different simulation scenarios at the CRP location. Spatial patterns of (estimated) soil properties and optimized irrigation

amounts for different simulation scenarios are also compared. This comparison is made at the scale of the complete CRP footprint. The temporal evolution of soil moisture content at 30 cm and 50 cm depth for different simulation scenarios is shown in Fig. 2. The scenario No_DA underestimated soil moisture content even although (too) high irrigation amounts were scheduled, which is related to the erroneous soil texture in this simulation scenario and the associated bias in soil properties like saturated hydraulic conductivity. In the data assimilation scenario Only_DA_SM soil moisture characterization was improved by assimilating the CRP neutron intensity, but the bias was also very high due to the large bias of soil properties. In order to reduce the soil moisture bias, the joint soil moisture state and bias estimation was evaluated in the scenario DA_SM_Bias by use of the state augmentation method. The soil moisture estimation became better than Only_DA_SM after the soil moisture bias was reduced. The best soil moisture results were obtained in the scenario DA_SM_Par, in which sand fraction, clay fraction and organic matter density were updated sequentially using the joint state and parameter estimation method.

[Insert Figure 2 here]

The RMSE values for soil moisture characterization are summarized in Fig. 3. Compared with the Reference scenario, the scenarios No_DA and Only_DA_SM underestimated soil moisture content, which resulted in higher irrigation requirement than for the reference case. Compared with the scenario No_DA, the RMSE values for soil moisture content at 30 cm depth decreased by 33%, 40% and 52% for the scenarios Only_DA_SM, DA_SM_Bias and DA_SM_Par, respectively. At 50cm

538 depth these RMSE-decreases were 39%, 35% and 51% for the scenarios
539 Only_DA_SM, DA_SM_Bias and DA_SM_Par, respectively. These results illustrate
540 the benefit of joint state-parameter estimation. Model results were strongly influenced
541 by the biased soil properties for the scenario Only_DA_SM, where measurement data
542 were not used to estimate model bias or soil properties. As model bias was related to
543 biased soil properties in these simulations, joint state and parameter estimation
544 performed better than the scenario with joint state and bias estimation.

545 [Insert Figure 3 here]

546 Fig. 4 shows the soil moisture bias for the different ensemble members (scenario
547 DA_SM_Bias). The temporal evolution of the bias is shown for the first soil layer and
548 the CRP location. The time series of true soil moisture bias (the scenario No_DA) is
549 shown for comparison. The mean bias value for No_DA is 0.051 m^3m^{-3} and 0.033
550 m^3m^{-3} for DA_SM_Bias. The joint state-bias estimation could reduce 35% of the soil
551 moisture bias introduced by the biased soil properties.

552 [Insert Figure 4 here]

553 The CLM model derives the soil hydraulic parameters using a predefined
554 pedotransfer function (Oleson et al., 2013). The updated soil texture resulted therefore
555 in updated soil hydraulic parameters in CLM. In order to show the influence of
556 calibrated soil texture on the soil hydraulic parameters, the temporal evolution of the
557 calibrated saturated hydraulic conductivity K and the empirical parameter B which
558 represent the slope of water retention curve in the Clapp–Hornberger parameterization
559 (Clapp and Hornberger, 1978; Oleson et al., 2013) are shown in Fig. 5 (scenario

560 DA_SM_Par). The Clapp–Hornberger parameterization can be used to calculate the
561 hydraulic conductivity when the soil water retention data are not available. All soil
562 hydraulic parameters could be improved in this scenario by assimilating the CRP
563 neutron intensity. The mean ensemble values for the soil hydraulic parameters
564 approached the reference values over the assimilation period. As the soil properties
565 were not updated during the intensive irrigation period, the convergence was slow.

566 [Insert Figure 5 here]

567 Fig. 6 shows the time series of irrigation amount at the location of the CRP for
568 the reference case and for the different estimation scenarios. The reference irrigation
569 amount (707.2 mm) was calculated in CLM on the basis of the water deficit method.
570 Fig. 6 illustrates that the intensive irrigation period from June to October coincided
571 with limited precipitation. The reference irrigation amount was around twice of the
572 annual precipitation amount (356.1 mm). The sum of the reference irrigation amount
573 (707.2 mm) and annual precipitation (356.1 mm) was about 6% higher than the
574 documented potential annual evapotranspiration of citrus trees (Ballester et al., 2011;
575 Jimenez-Bello et al., 2015). We used a t-test to compare the estimated annual
576 irrigation requirements by the different scenarios with the reference case. Large p
577 values (Fig. 6) indicate that the scenarios with data assimilation did not have a
578 significantly different irrigation scheduling as compared with the reference case. The
579 scenario No_DA has a p value <0.05, which indicates that the estimated irrigation
580 amounts were significantly different from the reference case. Data assimilation
581 (Only_DA_SM) improved results with higher p values ($p=0.205$). Scenarios with bias

582 correction (p=0.819) and parameter estimation (p=0.755) gave better results than the
583 scenario of state estimation only (Only_DA_SM). The annual irrigation amounts for
584 the grid cell at the location of the CRP are summarized in Fig. 7. Obviously, joint soil
585 moisture and bias (or parameter estimation) improved the characterization of
586 irrigation requirement.

587 [Insert Figure 6 here]

588 [Insert Figure 7 here]

589 Now we analyze the irrigation results for the scenarios in detail. The better
590 characterization of the irrigation demand was found by combining CRP neutron
591 intensity assimilation and soil properties estimation (or soil moisture bias estimation).
592 Scenarios DA_SM_Bias and DA_SM_Par estimated an irrigation requirement of
593 691.0 mm and 685.6 mm, respectively. The scenario Only_DA_SM (i.e., data
594 assimilation with state estimation only) gave an irrigation estimation of 797.7 mm.
595 CRP neutron intensity assimilation without parameter estimation provided much
596 better results than scenarios without data assimilation (No_DA). The estimated
597 irrigation amount for the scenario No_DA was 1107.3 mm. These results illustrate that
598 irrigation estimation for the case of biased soil properties (i.e., sandier soil in model
599 than in reference run) can be improved significantly by the assimilation of CRP
600 neutron intensity and even better by including soil properties estimation or bias
601 estimation. Data assimilation improved the estimation of irrigation demand and even
602 resulted in a slightly lower irrigation than for the reference case.

603 The CRP footprint was composed of 43 CLM grid cells which were irrigated

604 separately. The irrigation requirements estimated for the different scenarios are
605 displayed in Fig. 8 and compared with the reference scenario. The spatial irrigation
606 patterns of scenarios DA_SM_Bias and DA_SM_Par are closer to the reference case
607 than the scenario without data assimilation (No_DA).

608 [Insert Figure 8 here]

609 The single CRP neutron intensity measurement for the coarse scale (600 m) was
610 used to update the 43 CLM grid cells at the fine scale (100 m). The spatial distribution
611 of soil properties and annual irrigation amount were compared with the reference
612 spatial distributions. A higher spatial similarity is associated with lower HD values.
613 The HD values were evaluated according to the distance between a CLM grid cell and
614 the CRP location. Three classes were defined: (i) distance CRP- grid cell ≤ 100 m; (ii)
615 distance CRP- grid cell > 100 m and ≤ 200 m; (iii) distance CRP- grid cell > 200 m
616 and ≤ 300 m. The HD values for the comparison of the spatial patterns of soil
617 properties for the scenarios No_DA and DA_SM_Par are shown in Fig. 9. The
618 similarity of soil properties between background and reference is small due to the
619 imposed bias, and the HD values were 580.83, 1186.53, 1203.93 for sand fraction,
620 clay fraction and organic matter density, respectively. The scenario DA_SM_Par
621 resulted in a spatial distribution of soil properties closer to the reference case, with
622 HD values of 69.83 for sand fraction (580.83 for No_DA), 149.96 for clay fraction
623 (1186.53 for No_DA) and 185.21 for organic matter density (1203.93 for No_DA)
624 HD values for sand fraction, clay fraction and organic matter density for the region
625 with distance CRP- grid cell ≤ 100 m decreased by 80%, 82% and 64%, compared to

No_DA, respectively. For the region with distance CRP- grid cell > 100 m and ≤ 200 m the decreases were 82%, 66% and 67%, respectively. Finally, for the region with a distance CRP- grid cell > 200 m and ≤ 300 m the decreases were 78%, 82% and 40%, respectively.

Figure 10 shows the HD values for the comparison of the spatial distribution of irrigation amounts with the reference. The figure includes comparisons for all different data assimilation scenarios. It is clear that the assimilation of CRP neutron intensity (Only_DA_SM) increased the similarity between the spatial distribution of estimated annual irrigation amount and the reference irrigation distribution. Soil properties estimation and soil moisture bias estimation increased the similarity in spatial irrigation pattern further. The HD values for the scenario DA_SM_Bias decreased 89% (distance CRP- grid cell ≤ 100 m), 81% (distance CRP- grid cell > 100 m and ≤ 200 m) and 82% (distance CRP- grid cell > 200 m and ≤ 300 m) compared to No_DA. The HD values for the scenario DA_SM_Par, for the same three distance classes and in the same order, decreased by 88%, 87% and 85% compared to No_DA.

[Insert Figure 9 here]

[Insert Figure 10 here]

The total annual ET for the different scenarios was also calculated, and also the contributions from ground evaporation, evaporation of intercepted water by the canopy and canopy transpiration. The ET for the reference scenario was 756.6 mm. The ET for all other scenarios was very close to the reference. In case of the scenario No_DA, too much water was irrigated so that drought stress did not occur. The other

scenarios with data assimilation resulted in less irrigation, but ET was also close to the reference value, indicating that less irrigation was not associated with plant stress. For all the scenarios, the ET values did not deviate much from the reference value. This is because in all cases an overestimation of the percentage of sand led to excessive irrigation and sustainment of potential ET. The largest contribution to the ET was the canopy transpiration. The irrigated grid cells were assumed to be fully covered by the vegetation, and therefore the ground evaporation was low. The low evaporation from the canopy intercepted water maybe related to the fact that the rain events occurred mainly in the spring and winter seasons.

5. Discussion

The proposed data assimilation and parameter estimation (or bias estimation) can improve the soil moisture and irrigation estimation. The joint state-parameter estimation is the best scenario, and reduced the RMSE values of soil moisture content more than 50%, the spatial similarity of irrigation amount was increased and the HD values were decreased by 86% on average. The novelty of this work was the assimilation of the new CRP data in combination with irrigation scheduling. In general, classical parameter estimation tends to focus on uncertainty in the parameter estimates only, while neglecting partial or all of the other uncertainty sources (Liu and Gupta, 2007). We did not aim to compare the parameter estimation methodology with other methodologies in this study. The synthetic CRP neutron intensity observations were assimilated in CLM and the synthetic study potentially overestimated the

performance of the proposed method.

In a real-world application, the model will show systematical biases and also the implementation of the project area in the model is a strong simplification which might generate additional bias. A complication for the application of the data assimilation system in a real-world application is therefore the presence of model structural bias, and parameter estimation could compensate for this bias so that the estimated parameter values are not necessarily closer to the true parameter values. The approach will try to identify the effective parameter values that maximize model performance at that scale (Wagener et al., 2007). Therefore, as an alternative, instead of updating states and parameters jointly, also states and bias could be estimated jointly. It was shown in this paper that both approaches gave improvements. Although uncertainty of soil hydraulic parameters is important in the context of irrigation scheduling, it might be difficult to infer better estimates of soil hydraulic parameters due to other sources of uncertainty like model structural bias. On the other hand, this does not need to hamper successful operational implementation of the proposed method. Hendricks Franssen et al (2011) demonstrated the feasibility of operational prediction of groundwater levels (Franssen et al., 2011), coupled to operational optimization of groundwater management at the same site (Bauser et al., 2012). The water works Zurich applied this methodology (Franssen et al., 2011) now for the period 2009-2015, with consistent better predictions than for the open loop run. However, in the operational implementation on-line parameter estimation was avoided and only states were updated. It is therefore possible that for on-line irrigation scheduling a

692 conservative, potentially less successful strategy should be followed where only states
693 are updated. This synthetic study showed that state updating only also would improve
694 irrigation scheduling considerably. We believe therefore that although in a real-world
695 case study results will be less favorable than in the synthetic study, data assimilation
696 with updating states only, or joint updating of states and bias (or parameters) in case
697 of a systematic bias, will improve irrigation scheduling compared to a scenario
698 without data assimilation.

699 An additional challenge for the real world application is the forward modeling of
700 the CRP neutron intensity. The measured CRP neutron intensity needs to be corrected
701 for variations in the incoming high-energetic neutrons, the atmospheric pressure and
702 humidity, lattice water and organic carbon content of the soil, and aboveground
703 biomass. The aboveground biomass of citrus trees is temporally variable related to the
704 growth of the oranges (or lemons) over the year. The impact of vegetation water
705 content on the CRP neutron intensity is still under active study. In principle, an
706 empirical methodology is suited to correct for the influence of aboveground biomass
707 on measured neutron count intensity (Baatz et al., 2015). In this study, the
708 synthetically measured CRP neutron intensity was applied uniformly at the CRP
709 footprint and a simple multiscale data assimilation scheme was proposed to update the
710 field scale CLM simulation using coarse scale CRP neutron intensity. This may not be
711 optimal as all the grid cells within the CRP footprint contribute differently to the
712 measured CRP neutron intensity. The soil spatial heterogeneity in the CRP footprint
713 was introduced by adding a random spatially correlated noise. Heterogeneous land

cover was not considered in this study. However, the spatial variability of ecosystem parameters could be a further confounding parameter influencing the results. Altogether, accounting for temporally variable biomass in the COSMIC operator does not seem a large limitation, but spatially variable soil moisture conditions within the cosmic ray probe footprint, are a serious challenge.

Furthermore, the weather forecast is essential to the irrigation scheduling. This aspect was not considered in this work. If the precise precipitation forecast cannot be obtained, the irrigation requirement cannot be estimated accurately.

A further important complication for real-world applications is that farmers want to irrigate the citrus based on their own experience, and in combination with the low water prices they might not want to follow the suggested irrigation scheduling. Altogether, we feel that the methodology is suited for real-world applications and can improve irrigation scheduling compared to more traditional scheduling, but that the farmer participation is the most critical factor, besides model structural bias and soil moisture heterogeneity within the cosmic ray probe footprint.

Therefore, the successful real application of the proposed method needs: a calibrated land surface model, an improved COSMIC operator in which the measured cosmic-ray neutron intensity is corrected for above and below ground biomass, not too large spatial variability of soil moisture content within the cosmic ray probe footprint and a precise weather forecast including uncertainty characterization and participation of farmers.

A further possible improvement is the consideration of irrigation below ET

736 requirement, known as deficit irrigation (DI), which can reduce water demand to meet
737 the maximum ET (Fereres and Soriano, 2007).
738
739 **6. Conclusions**
740 This study investigated the assimilation of synthetic measurements of coarse
741 scale CRP neutron intensity in CLM for updating field scale root zone soil moisture
742 content. The synthetic study mimicked a drip irrigated citrus farmland near Valencia,
743 Spain. CLM was driven by biased soil properties and the joint estimation of soil
744 moisture and soil properties (or soil moisture bias) was evaluated in a data
745 assimilation framework using the state augmentation method. The non-linear
746 measurement operator COSMIC was used to simulate the CRP neutron intensity on
747 the basis of the soil moisture profile estimated by the CLM model. Fast neutron
748 intensity was assimilated directly, and both soil moisture and soil properties (soil
749 moisture bias) were updated using the LETKF in combination with the CLM model.
750 The horizontal and vertical weights for the different CLM grid cells in the CRP
751 footprint were also considered using a Gaussian window function.
752 The results show that assimilating CRP neutron intensity can improve joint soil
753 moisture and soil properties estimation, and irrigation scheduling. Data assimilation
754 schemes that remove soil moisture bias or update soil properties on the basis of CRP
755 neutron intensity outperform data assimilation without bias or parameter estimation.
756 The joint soil moisture and soil parameter estimation with simple multiscale
757 assimilation strategy of CRP neutron intensity can potentially be used for irrigation

scheduling in the future. The main challenges for the real world application are: model calibration to remove the bias, forward modeling of cosmic-ray neutron intensity under high vegetation coverage, precise weather forecasts and cooperation of farmers.

Acknowledgments

This work was supported by AGADAPT (adapting water use by the agriculture sector) financed by Climate Knowledge and Innovation Community (Climate-KIC) of the European Union. AGADAPT focuses on the development and deployment of novel methods to reduce and optimize the water usage of rain-fed and irrigated agriculture by combining knowledge-based innovative technologies, modelling and transfer of technologies and innovative practices. The work was also supported by Transregional Collaborative Research Centre 32, and the NSFC project (grant number: 41271357, 91125001). The support of the supercomputing facilities of Forschungszentrum Julich (JUROPA) is gratefully acknowledged.

References:

Aravéquia, J.A. et al., 2011. Evaluation of a Strategy for the Assimilation of Satellite Radiance Observations with the Local Ensemble Transform Kalman Filter. Mon Weather Rev, 139(6): 1932-1951.

Baatz, R. et al., 2015. An empirical vegetation correction for soil water content quantification using cosmic ray probes. Water Resour Res, 51(4): 2030-2046.

Baek, S.J., Hunt, B.R., Kalnay, E., Ott, E., Szunyogh, I., 2006. Local ensemble Kalman filtering in the presence of model bias. Tellus A, 58(3): 293-306.

Ballester, C., Castel, J., Intrigliolo, D.S., Castel, J.R., 2011. Response of Clementina de Nules citrus trees to summer deficit irrigation. Yield components and fruit composition. Agr Water Manage, 98(6): 1027-1032.

Bateni, S.M., Entekhabi, D., 2012. Surface heat flux estimation with the ensemble Kalman smoother: Joint estimation of state and parameters. Water Resour Res, 48.

Bauser, G. et al., 2012. A comparison study of two different control criteria for the real-time management of urban groundwater works. J Environ Manage, 105: 21-9.

Bogena, H.R., Huisman, J.A., Baatz, R., Hendricks Franssen, H.J., Vereecken, H., 2013. Accuracy of the cosmic-ray soil water content probe in humid forest ecosystems: The worst case scenario. Water Resour Res, 49(9): 5778-5791.

Bosilovich, M.G., Radakovich, J.D., da Silva, A., Todling, R., Verter, F., 2007. Skin temperature analysis and bias correction in a coupled land-atmosphere data assimilation system. J Meteorol Soc Jpn, 85A: 205-228.

Chen, Y., Zhang, D.X., 2006. Data assimilation for transient flow in geologic formations via ensemble Kalman filter. Adv Water Resour, 29(8): 1107-1122.

Clapp, R.B., Hornberger, G.M., 1978. Empirical equations for some soil hydraulic properties. Water Resour Res, 14(4): 601-604.

Crow, W.T. et al., 2012. Upscaling Sparse Ground-Based Soil Moisture Observations for the Validation of Coarse-Resolution Satellite Soil Moisture Products. Rev Geophys, 50(2): n/a-n/a.

Crow, W.T., Kustas, W.P., Prueger, J.H., 2008. Monitoring root-zone soil moisture through the assimilation of a thermal remote sensing-based soil moisture proxy into a water balance model. Remote Sens Environ, 112(4): 1268-1281.

De Lannoy, G.J.M., Houser, P.R., Pauwels, V.R.N., Verhoest, N.E.C., 2007a. State and bias estimation for soil moisture profiles by an ensemble Kalman filter: Effect of assimilation depth and frequency. Water Resour Res, 43(6).

De Lannoy, G.J.M., Reichle, R.H., Houser, P.R., Pauwels, V.R.N., Verhoest, N.E.C., 2007b. Correcting for forecast bias in soil moisture assimilation with the ensemble Kalman filter. Water Resour Res, 43(9): n/a-n/a.

Dee, D.P., 2005. Bias and data assimilation. Q J Roy Meteor Soc, 131(613): 3323-3343.

Desilets, D., Zreda, M., Ferre, T.P.A., 2010. Nature's neutron probe: Land surface hydrology at an elusive scale with cosmic rays. Water Resour Res, 46(11): W11505.

Entekhabi, D. et al., 2010. The Soil Moisture Active Passive (SMAP) Mission. P Ieee, 98(5): 704-716.

Fereres, E., Soriano, M.A., 2007. Deficit irrigation for reducing agricultural water use. J Exp Bot, 58(2): 147-159.

Franssen, H.J.H. et al., 2011. Operational real-time modeling with ensemble Kalman filter of variably

817 saturated subsurface flow including stream-aquifer interaction and parameter updating.
818 Water Resour Res, 47(2): n/a-n/a.
819 Franssen, H.J.H., Kinzelbach, W., 2008. Real-time groundwater flow modeling with the Ensemble
820 Kalman Filter: Joint estimation of states and parameters and the filter inbreeding problem.
821 Water Resour Res, 44(9): W09408.
822 Franz, T.E., Zreda, M., Rosolem, R., Ferre, T.P.A., 2013. A universal calibration function for
823 determination of soil moisture with cosmic-ray neutrons. Hydrology and Earth System
824 Sciences, 17(2): 453-460.
825 Greybush, S.J., Kalnay, E., Miyoshi, T., Ide, K., Hunt, B.R., 2011. Balance and Ensemble Kalman Filter
826 Localization Techniques. Mon Weather Rev, 139(2): 511-522.
827 Han, X. et al., 2015a. Correction of systematic model forcing bias of CLM using assimilation of
828 cosmic-ray Neutrons and land surface temperature: a study in the Heihe Catchment, China.
829 Hydrology and Earth System Sciences, 19(1): 615-629.
830 Han, X., Li, X., Franssen, H.J.H., Vereecken, H., Montzka, C., 2012. Spatial horizontal correlation
831 characteristics in the land data assimilation of soil moisture. Hydrology and Earth System
832 Sciences, 16(5): 1349-1363.
833 Han, X., Li, X., Rigon, R., Jin, R., Endrizzi, S., 2015b. Soil moisture estimation by assimilating L-band
834 microwave brightness temperature with geostatistics and observation localization. Plos One,
835 10(1): e0116435.
836 Han, X.J. et al., 2013. Joint Assimilation of Surface Temperature and L-Band Microwave Brightness
837 Temperature in Land Data Assimilation. Vadose Zone J, 12(3): 0.
838 Han, X.J., Franssen, H.J.H., Montzka, C., Vereecken, H., 2014a. Soil moisture and soil properties
839 estimation in the Community Land Model with synthetic brightness temperature
840 observations. Water Resour Res, 50(7): 6081-6105.
841 Han, X.J., Jin, R., Li, X., Wang, S.G., 2014b. Soil Moisture Estimation Using Cosmic-Ray Soil Moisture
842 Sensing at Heterogeneous Farmland. Ieee Geoscience and Remote Sensing Letters, 11(9):
843 1659-1663.
844 Harris, F.J., 1978. On the use of windows for harmonic analysis with the discrete Fourier transform. P
845 Ieee, 66(1): 51-83.
846 Hendrick, L.D., Edge, R.D., 1966. Cosmic-Ray Neutrons near the Earth. Physical Review, 145(4):
847 1023-1025.
848 Heng, L.K., Hsiao, T., Evett, S., Howell, T., Steduto, P., 2009. Validating the FAO AquaCrop Model for
849 Irrigated and Water Deficient Field Maize. Agron J, 101(3): 488-498.
850 Hou, Z.S., Huang, M.Y., Leung, L.R., Lin, G., Ricciuto, D.M., 2012. Sensitivity of surface flux simulations
851 to hydrologic parameters based on an uncertainty quantification framework applied to the
852 Community Land Model. J Geophys Res-Atmos, 117.
853 Huang, C.L., Li, X., Lu, L., Gu, J., 2008. Experiments of one-dimensional soil moisture assimilation
854 system based on ensemble Kalman filter. Remote Sens Environ, 112(3): 888-900.
855 Hunt, B.R., Kostelich, E.J., Szunyogh, I., 2007. Efficient data assimilation for spatiotemporal chaos: A
856 local ensemble transform Kalman filter. Physica D: Nonlinear Phenomena, 230(1-2): 112-126.
857 Jimenez-Bello, M.A., Castel, J.R., Testi, L., Intrigliolo, D.S., 2015. Assessment of a Remote Sensing
858 Energy Balance Methodology (SEBAL) Using Different Interpolation Methods to Determine
859 Evapotranspiration in a Citrus Orchard. Ieee J-Stars, 8(4): 1465-1477.
860 Kerr, Y.H. et al., 2010. The SMOS Mission: New Tool for Monitoring Key Elements ofthe Global Water

Cycle. P Ieee, 98(5): 666-687.
Kumar, S.V. et al., 2012a. Land surface Verification Toolkit (LVT) – a generalized framework for land surface model evaluation. Geosci Model Dev, 5(3): 869-886.
Kumar, S.V. et al., 2012b. A comparison of methods for a priori bias correction in soil moisture data assimilation. Water Resour Res, 48(3): n/a-n/a.
Kumar, S.V., Reichle, R.H., Koster, R.D., Crow, W.T., Peters-Lidard, C.D., 2009. Role of Subsurface Physics in the Assimilation of Surface Soil Moisture Observations. J Hydrometeorol, 10(6): 1534-1547.
Kurtz, W., Hendricks Franssen, H.J., Kaiser, H.P., Vereecken, H., 2014. Joint assimilation of piezometric heads and groundwater temperatures for improved modeling of river-aquifer interactions. Water Resour Res, 50(2): 1665-1688.
Lal, D., Peters, B., 1967. Cosmic Ray Produced Radioactivity on the Earth. In: Sitte, K. (Ed.), Kosmische Strahlung II / Cosmic Rays II. Handbuch der Physik / Encyclopedia of Physics. Springer Berlin Heidelberg, pp. 551-612.
Levis, S., Sacks, W.J., 2011. Technical descriptions of the interactive crop management (CLM4CNcrop) and interactive irrigation models in version 4 of the Community Land Model. [Available online at http://www.cesm.ucar.edu/models/cesm1.0/clm/index.shtml.].
Li, C., Ren, L., 2011. Estimation of Unsaturated Soil Hydraulic Parameters Using the Ensemble Kalman Filter. Vadose Zone J, 10(4): 1205.
Lien, G.Y., Kalnay, E., Miyoshi, T., 2013. Effective assimilation of global precipitation: simulation experiments. Tellus A, 65(0).
Liu, Y.Q., Gupta, H.V., 2007. Uncertainty in hydrologic modeling: Toward an integrated data assimilation framework. Water Resour Res, 43(7): n/a-n/a.
Merlin, O., Walker, J.P., Panciera, R., Escorihuela, M.J., Jackson, T.J., 2009. Assessing the SMOS Soil Moisture Retrieval Parameters With High-Resolution NAFE'06 Data. Ieee Geoscience and Remote Sensing Letters, 6(4): 635-639.
Miyoshi, T., Kondo, K., Imamura, T., 2014. The 10,240-member ensemble Kalman filtering with an intermediate AGCM. Geophys Res Lett, 41(14): 5264-5271.
Miyoshi, T., Yamane, S., 2007. Local Ensemble Transform Kalman Filtering with an AGCM at a T159/L48 Resolution. Mon Weather Rev, 135(11): 3841-3861.
Montzka, C. et al., 2013. Brightness Temperature and Soil Moisture Validation at Different Scales During the SMOS Validation Campaign in the Rur and Erft Catchments, Germany. Ieee T Geosci Remote, 51(3): 1728-1743.
Montzka, C. et al., 2011. Hydraulic parameter estimation by remotely-sensed top soil moisture observations with the particle filter. Journal of Hydrology, 399(3-4): 410-421.
Moradkhani, H., Hsu, K.-L., Gupta, H., Sorooshian, S., 2005a. Uncertainty assessment of hydrologic model states and parameters: Sequential data assimilation using the particle filter. Water Resour Res, 41(5): n/a-n/a.
Moradkhani, H., Sorooshian, S., Gupta, H.V., Houser, P.R., 2005b. Dual state－parameter estimation of hydrological models using ensemble Kalman filter. Adv Water Resour, 28(2): 135-147.
Njoku, E.G., Chan, S.K., 2006. Vegetation and surface roughness effects on AMSR-E land observations. Remote Sens Environ, 100(2): 190-199.
Oleson, K. et al., 2013. Technical Description of version 4.5 of the Community Land Model (CLM). Ncar Technical Note NCAR/TN-503+STR, National Center for Atmospheric Research, Boulder, CO, 422 pp.

905 Park, S.K., Xu, L., 2009. Data assimilation for atmospheric, oceanic and hydrologic applications.
906 Springer, Berlin/Heidelberg, 730 pp.
907 Pauwels, V.R.N. et al., 2009. Optimization of Soil Hydraulic Model Parameters Using Synthetic Aperture
908 Radar Data: An Integrated Multidisciplinary Approach. Ieee T Geosci Remote, 47(2): 455-467.
909 Reichle, R.H., Crow, W.T., Koster, R.D., Sharif, H.O., Mahanama, S.P.P., 2008. Contribution of soil
910 moisture retrievals to land data assimilation products. Geophys Res Lett, 35(1).
911 Reichle, R.H., Kumar, S.V., Mahanama, S.P.P., Koster, R.D., Liu, Q., 2010. Assimilation of
912 Satellite-Derived Skin Temperature Observations into Land Surface Models. J Hydrometeorol,
913 11(5): 1103-1122.
914 Rosolem, R., Gupta, H.V., Shuttleworth, W.J., Zeng, X., de Gonçalves, L.G.G., 2012. A fully
915 multiple-criteria implementation of the Sobol′ method for parameter sensitivity analysis.
916 Journal of Geophysical Research: Atmospheres, 117(D7): D07103.
917 Rosolem, R. et al., 2014. Translating aboveground cosmic-ray neutron intensity to high-frequency soil
918 moisture profiles at sub-kilometer scale. Hydrology and Earth System Sciences, 18(11):
919 4363-4379.
920 Rosolem, R. et al., 2013. The Effect of Atmospheric Water Vapor on Neutron Count in the Cosmic-Ray
921 Soil Moisture Observing System. J Hydrometeorol, 14(5): 1659-1671.
922 Ruiz, J.J., Pulido, M., Miyoshi, T., 2013. Estimating Model Parameters with Ensemble-Based Data
923 Assimilation: A Review. J Meteorol Soc Jpn, 91(2): 79-99.
924 Sampathkumar, T., Pandian, B.J., Mahimairaja, S., 2012. Soil moisture distribution and root characters
925 as influenced by deficit irrigation through drip system in cotton-maize cropping sequence. Agr
926 Water Manage, 103: 43-53.
927 Schöniger, A., Nowak, W., Hendricks Franssen, H.J., 2012. Parameter estimation by ensemble Kalman
928 filters with transformed data: Approach and application to hydraulic tomography. Water
929 Resour Res, 48(4): n/a-n/a.
930 Schwinger, J., Kollet, S.J., Hoppe, C.M., Elbern, H., 2010. Sensitivity of Latent Heat Fluxes to Initial
931 Values and Parameters of a Land-Surface Model. Vadose Zone J, 9(4): 984-1001.
932 Shuttleworth, J., Rosolem, R., Zreda, M., Franz, T.E., 2013. The COsmic-ray Soil Moisture Interaction
933 Code (COSMIC) for use in data assimilation. Hydrology and Earth System Sciences, 17(8):
934 3205-3217.
935 Velikova, V. et al., 2012. The impact of winter flooding with saline water on foliar carbon uptake and
936 the volatile fraction of leaves and fruits of lemon (Citrus×limon) trees. Functional Plant
937 Biology, 39(3): 199.
938 Vrugt, J.A., Diks, C.G.H., Gupta, H.V., Bouten, W., Verstraten, J.M., 2005. Improved treatment of
939 uncertainty in hydrologic modeling: Combining the strengths of global optimization and data
940 assimilation. Water Resour Res, 41(1).
941 Vrugt, J.A., Gupta, H.V., Nuallain, B.O., 2006. Real-time data assimilation for operational ensemble
942 streamflow forecasting. J Hydrometeorol, 7(3): 548-565.
943 Wagener, T., Sivapalan, M., Troch, P., Woods, R., 2007. Catchment Classification and Hydrologic
944 Similarity. Geography Compass, 1(4): 901-931.
945 Walker, J.P., Willgoose, G.R., Kalma, J.D., 2001. One-dimensional soil moisture profile retrieval by
946 assimilation of near-surface observations: a comparison of retrieval algorithms. Adv Water
947 Resour, 24(6): 631-650.
948 Waller, J.A., Dance, S.L., Lawless, A.S., Nichols, N.K., Eyre, J.R., 2014. Representativity error for

temperature and humidity using the Met Office high-resolution model†. Q J Roy Meteor Soc, 140(681): 1189-1197.

Wanders, N., Bierkens, M.F.P., de Jong, S.M., de Roo, A., Karssenberg, D., 2014. The benefits of using remotely sensed soil moisture in parameter identification of large-scale hydrological models. Water Resour Res, 50(8): 6874-6891.

Welch, B.L., 1947. The Generalization of Students Problem When Several Different Population Variances Are Involved. Biometrika, 34(1-2): 28-35.

Wood, E.F. et al., 2011. Hyperresolution global land surface modeling: Meeting a grand challenge for monitoring Earth's terrestrial water. Water Resour Res, 47(5): W05301.

Wu, C.-C., Margulis, S.A., 2013. Real-Time Soil Moisture and Salinity Profile Estimation Using Assimilation of Embedded Sensor Datastreams. Vadose Zone J, 12(1): 0.

Zeng, X.B., 2001. Global vegetation root distribution for land modeling. J Hydrometeorol, 2(5): 525-530.

Zreda, M., Desilets, D., Ferre, T.P.A., Scott, R.L., 2008. Measuring soil moisture content non-invasively at intermediate spatial scale using cosmic-ray neutrons. Geophys Res Lett, 35(21): L21402.

Zreda, M. et al., 2012. COSMOS: the COsmic-ray Soil Moisture Observing System. Hydrology and Earth System Sciences, 16(11): 4079-4099.

Table List

971 Table 1 Summary of perturbation parameters for atmospheric forcing data

Variables	**Noise**	**Standard deviation**	**Time Correlation scale**	**Forcing Cross Correlation**
Precipitation	Multiplicative	0.5	24 h	[1.0,-0.8, 0.5, 0.0,
Shortwave radiation	Multiplicative	0.3	24 h	-0.8, 1.0,-0.5, 0.4,
Longwave radiation	Additive	20 W/m^2	24 h	0.5, -0.5, 1.0, 0.4,
Air temperature	Additive	1 K	24 h	0.0, 0.4, 0.4, 1.0]

972

973

Figure List

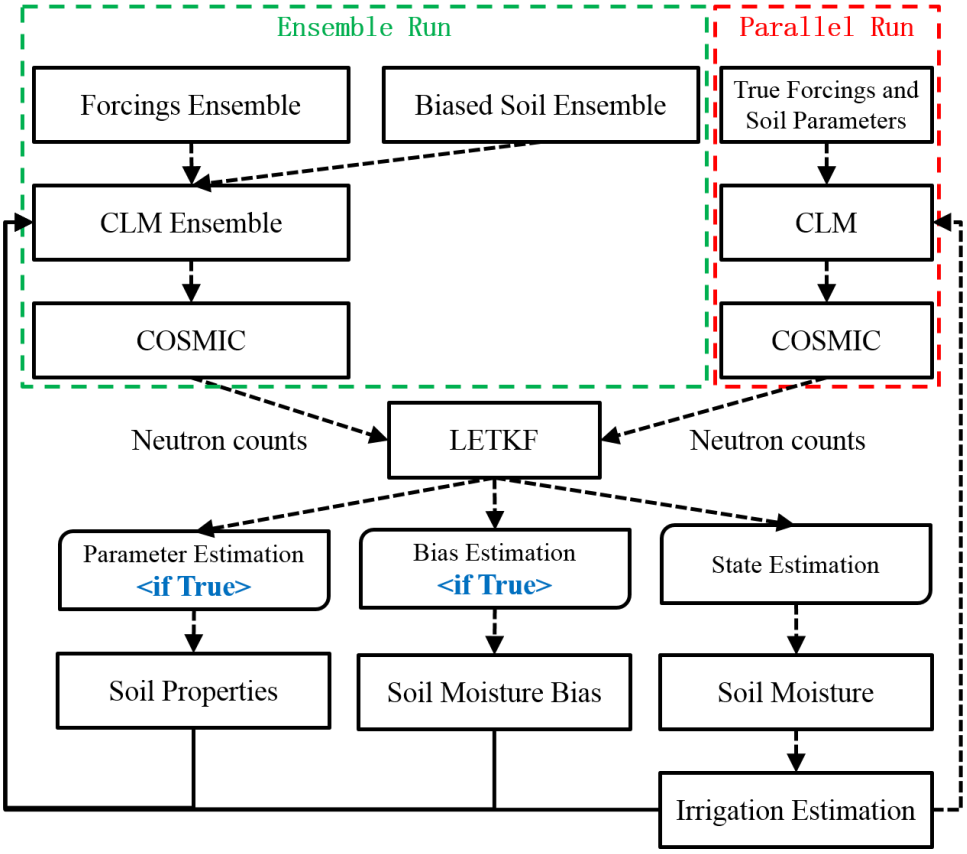

Figure 1. Schematic overview of the different steps of the irrigation optimization procedure

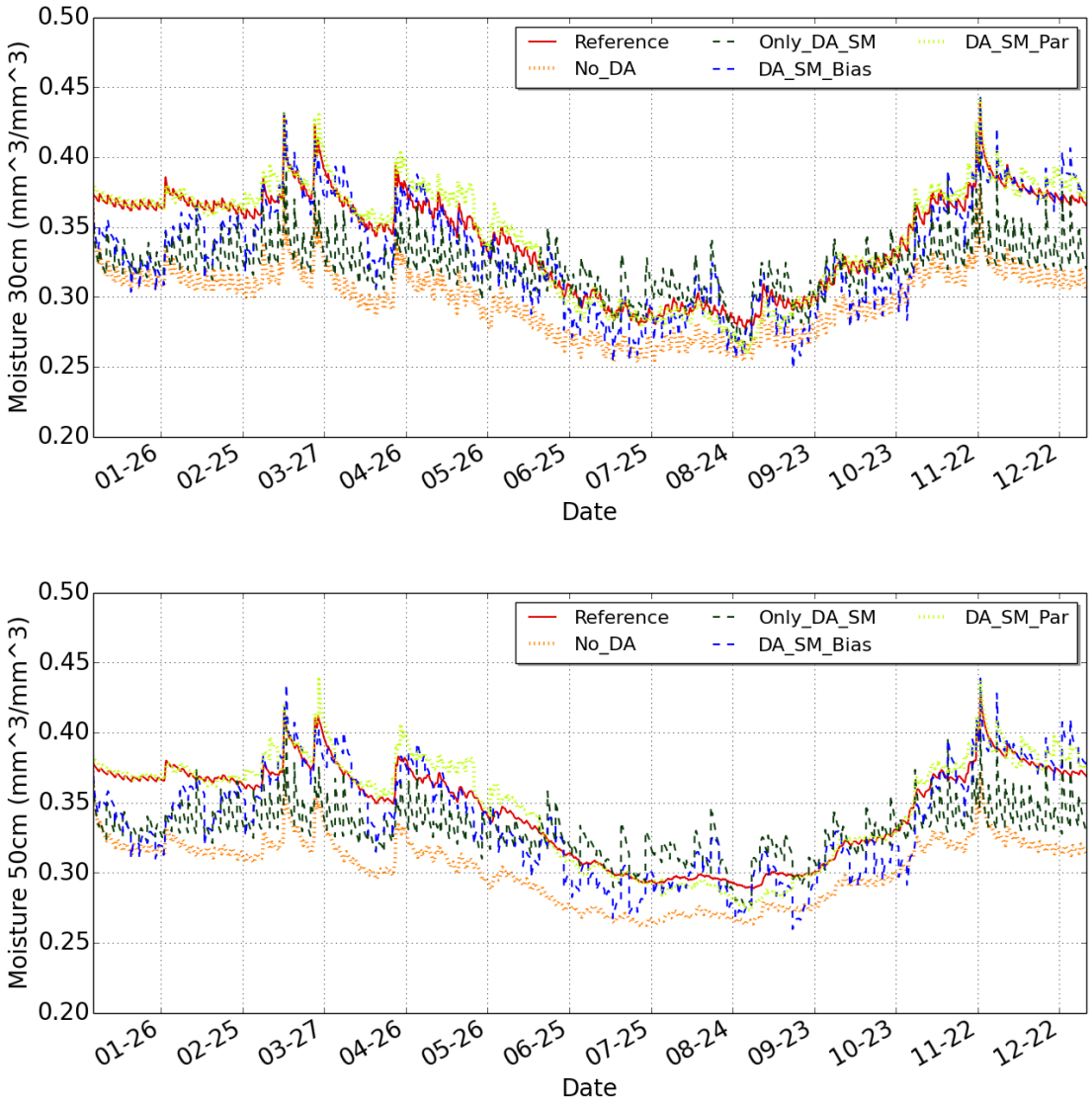

Figure 2. Soil moisture content at 30 cm (upper graph) and 50 cm (lower graph) depth at the CRP location for the different simulation scenarios

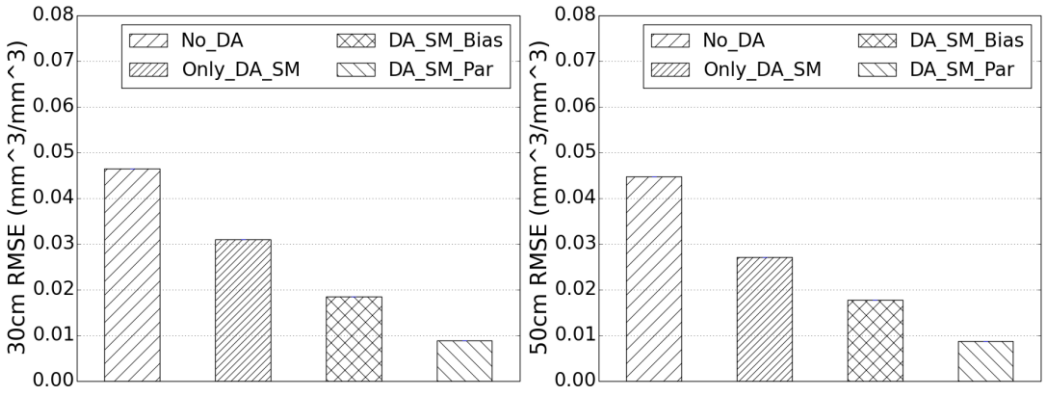

Figure 3. RMSE values for soil moisture content at 30 cm depth (left graph) and 50 cm depth (right graph) for the different scenarios at the CRP location

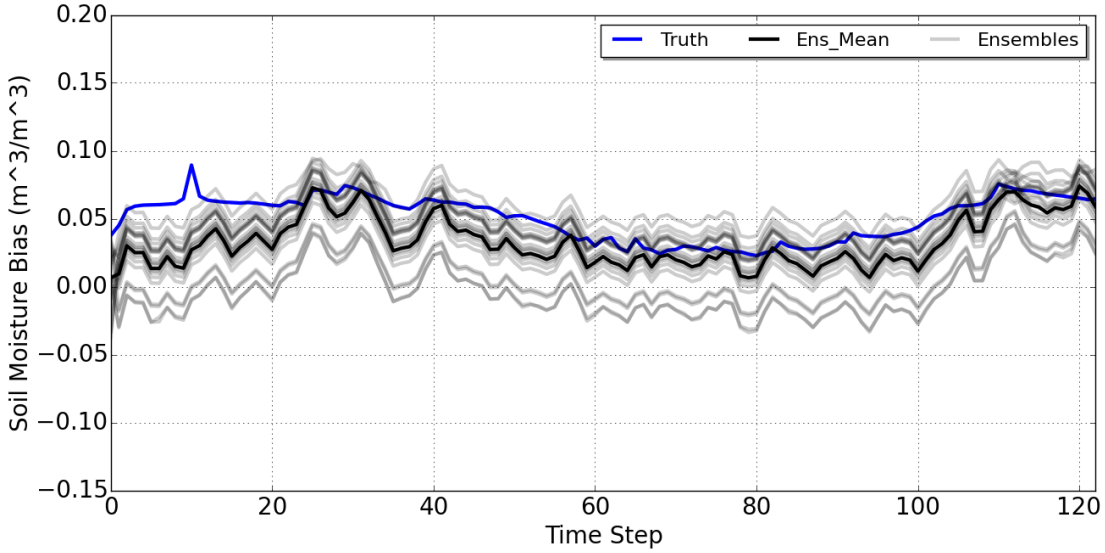

Figure 4. Temporal evolution (collected every three days) of soil moisture bias for the first soil layer at the CRP location (scenario DA_SM_Bias). The true soil moisture bias was calculated from the scenario No_DA and is shown in blue. The unit of x-axis is for time steps of 3 days.

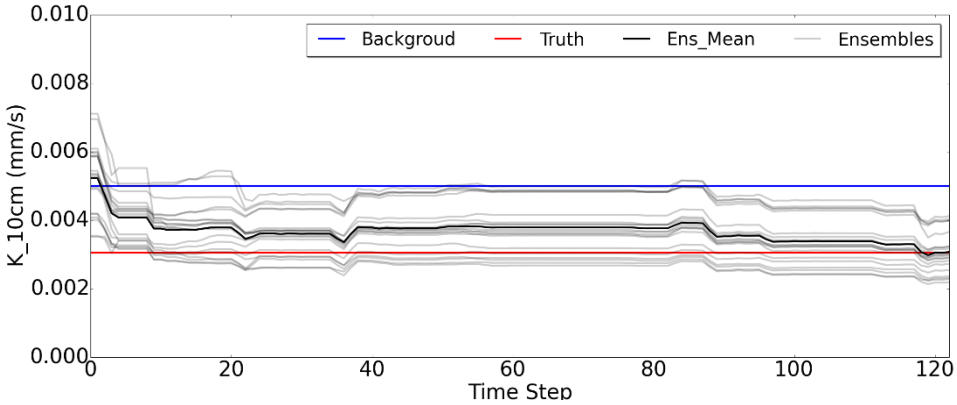

1022

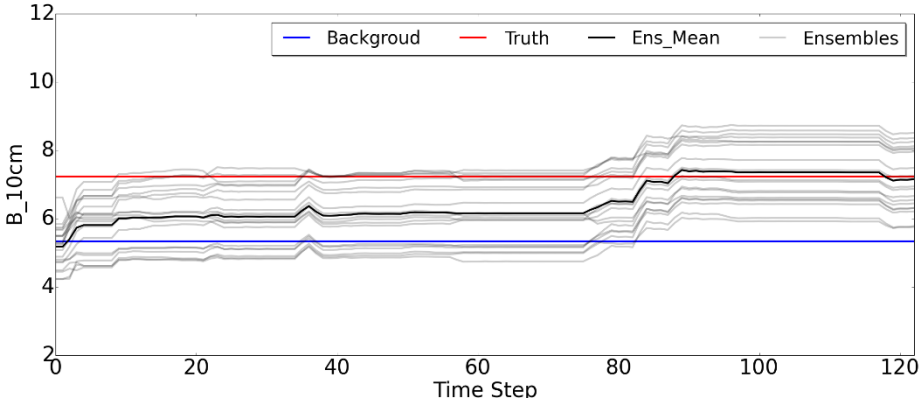

1023

1024 Figure 5. Temporal evolution (collected every three days) of saturated hydraulic
1025 conductivity *K* of soil (K_10cm) and the empirical parameter *B* of the Clapp–
1026 Hornberger parameterization (B_10cm) at the CRP location for the scenario
1027 DA_SM_Par. The unit of x-axis is for time steps of 3 days.

1028

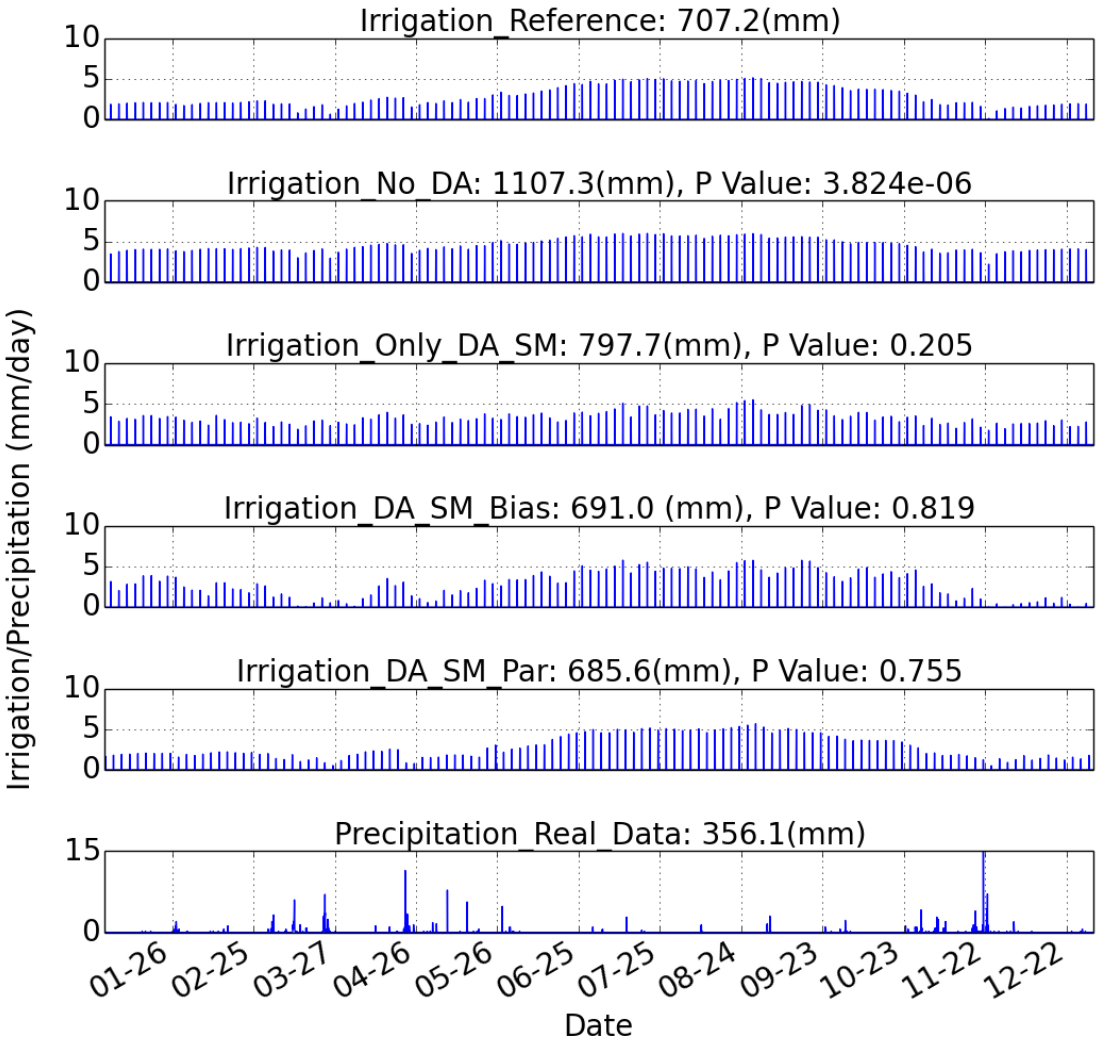

Figure 6. Irrigation requirement as function of time at the CRP location for the different scenarios; t-test statistics (p-value) with significance level 0.05 for comparing the calculated irrigation distribution with reference irrigation are also shown for the different scenarios (large p-values indicate high similarity)

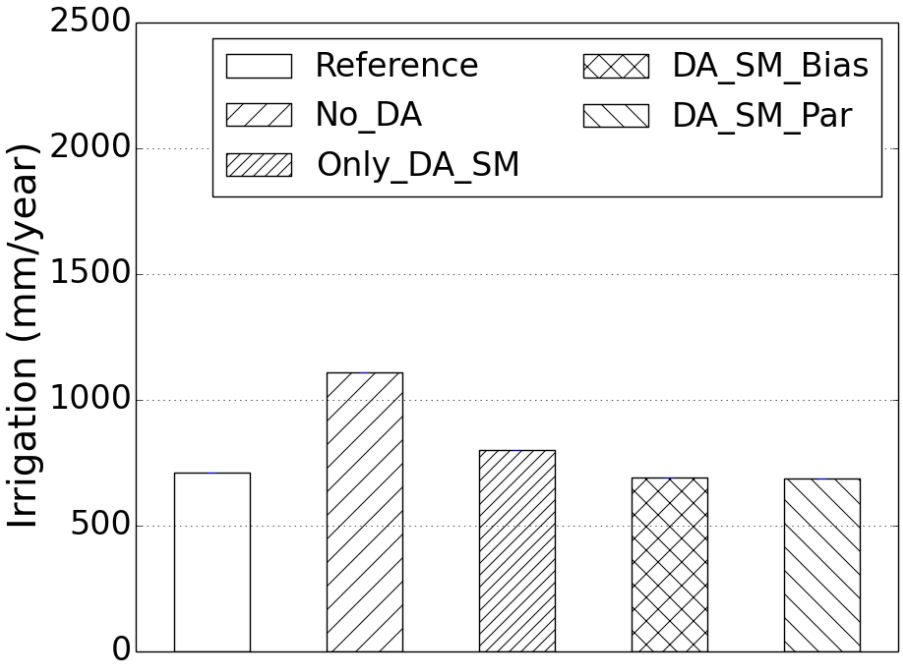

Figure 7. Annual irrigation requirement according to the different scenarios at the CRP location

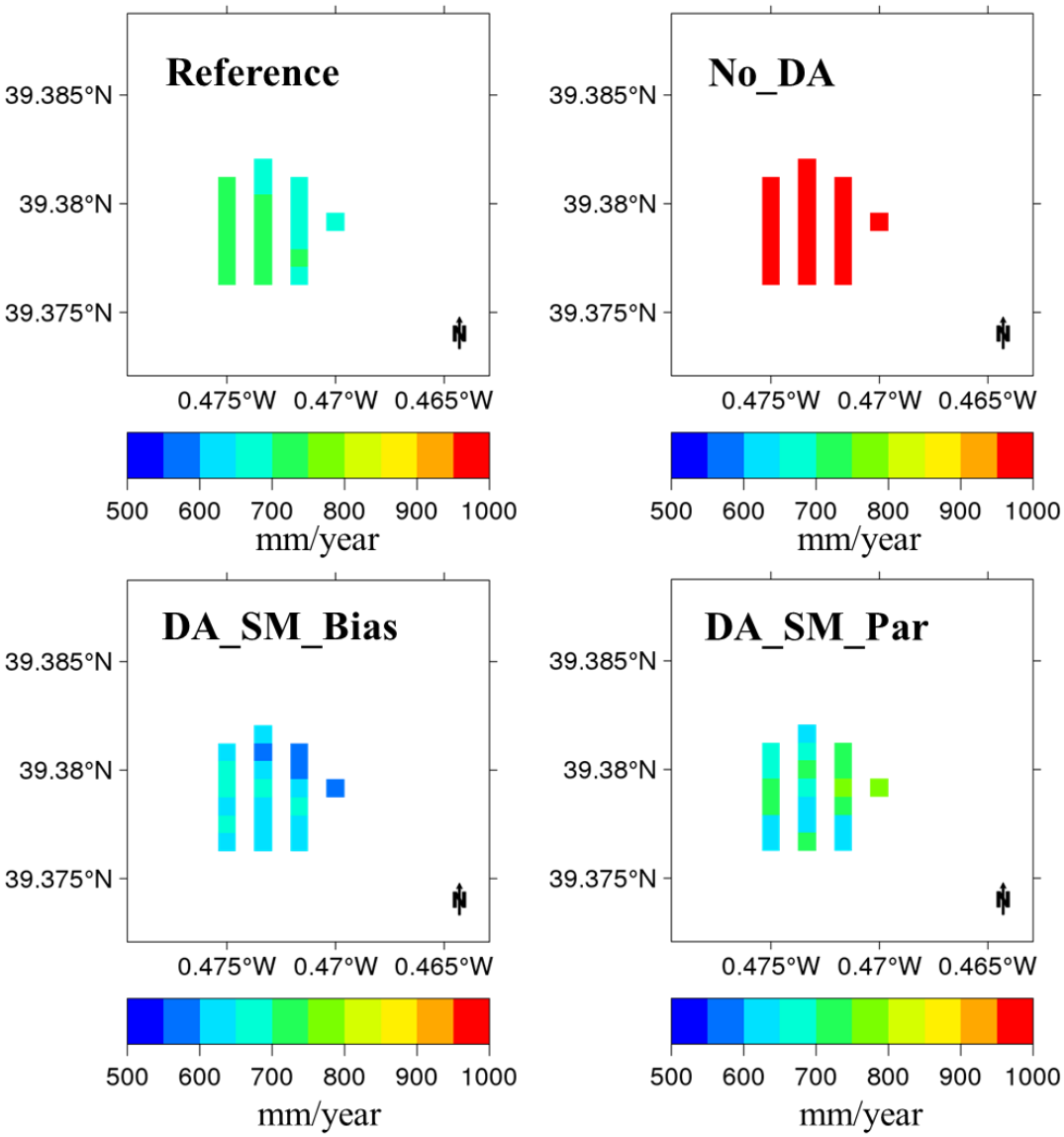

Figure 8. Annual irrigation calculated for different simulations scenarios and compared to the reference scenario

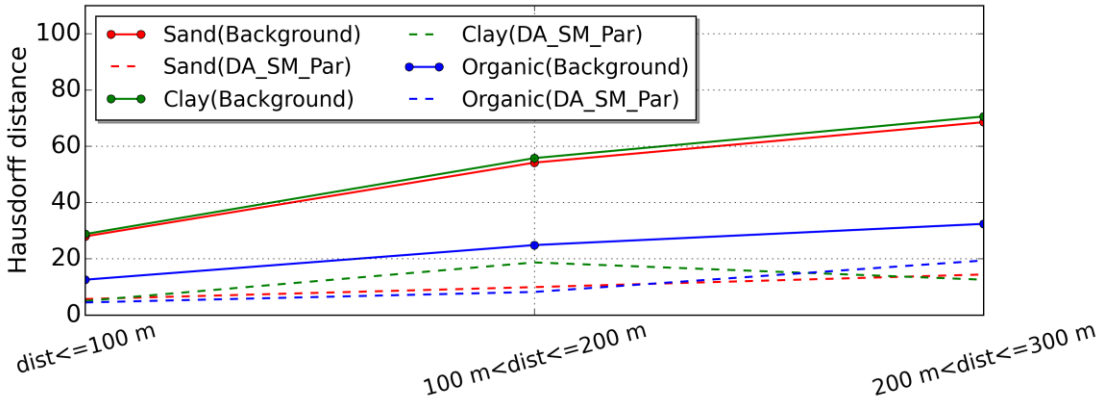

Figure 9. Hausdorff distance values for background soil properties (sand fraction, clay fraction and organic matter density) and estimated soil properties (scenario DA_SM_Par). Results are plotted as function of the distance between model grid cells and the CRP location

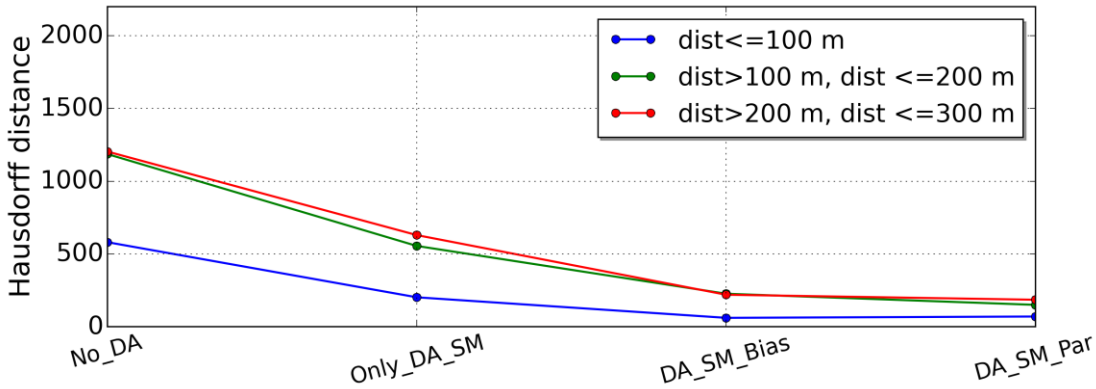

Figure 10. Hausdorff distance values of calculated annual irrigation requirement, compared to reference irrigation, for different scenarios. Results are plotted as function of distance between model grid cells and CRP location